NAVAL POSTGRADUATE SCHOOL
Monterey, California

THESIS

TURBULENCE PROFILES AND OUTER
LENGTH SCALE DETERMINATION IN THE
ATMOSPHERE USING BALLOONS

by

Aaron M. Holdaway

March 2000

Thesis Advisor:	Donald L. Walters
Co-Advisor:	Douglas K. Miller

Approved for public release; distribution is unlimited.

1. AGENCY USE ONLY *(Leave blank)*	2. REPORT DATE March 2000	3. REPORT TYPE AND DATES COVERED Master's Thesis

4. TITLE AND SUBTITLE **Turbulence Profiles And Outer Length Scale Determination In The Atmosphere Using Balloons**	5. FUNDING NUMBERS
6. AUTHOR(S) Holdaway, Aaron M.	

7. PERFORMING ORGANIZATION NAME(S) AND ADDRESS(ES) Naval Postgraduate School Monterey, CA 93943-5000	8. PERFORMING ORGANIZATION REPORT NUMBER

9. SPONSORING / MONITORING AGENCY NAME(S) AND ADDRESS(ES)	10. SPONSORING / MONITORING AGENCY REPORT NUMBER

11. SUPPLEMENTARY NOTES
The views expressed in this thesis are those of the author and do not reflect the official policy or position of the Department of Defense or the U.S. Government.

12a. DISTRIBUTION / AVAILABILITY STATEMENT Approved for public release; distribution is unlimited.	12b. DISTRIBUTION CODE

13. ABSTRACT

Turbulence in the atmosphere drives the formation of temperature inhomogeneities that scatter and diffract propagating electromagnetic waves, adversely affecting laser weapons and high-resolution optical systems. Military operations require reliable turbulence profiles for the development and validation of turbulence prediction models.

This research investigated the false turbulence contribution caused by well-known temperature steps in the vertical profile of the atmosphere, especially in the stratosphere. The homogeneity and isotropy requirements of structure functions were used to develop a technique to remove the false contribution to the temperature structure constant, c_T^2.

Both 1.54 cm and 5.82 m vertical resolution profiles with 0.001 to 0.01 K temperature resolution were collected from a balloon flight. Steps of 0.1 to 1 K in the vertical temperature profile produce abrupt changes in the mean temperature that obscure the measurement of the actual turbulent fluctuations. Removing these anomalies exposed the underlying c_T^2 distribution. Application of the new technique for several sampling intervals revealed a Kolmogorov inertial subrange extending from ~25 cm to ~10 m. The potential of this technique to compute the isoplanatic angle, θ_0, coherence length, r_0, and Greenwood frequency, f_g, reliably by using inexpensive balloons should benefit airborne and space-based laser programs.

14. SUBJECT TERMS Adaptive, Atmosphere, Laser, Optics, Propagation, Turbulence			15. NUMBER OF PAGES 62
			16. PRICE CODE

17. SECURITY CLASSIFICATION OF REPORT Unclassified	18. SECURITY CLASSIFICATION OF THIS PAGE Unclassified	19. SECURITY CLASSIFICATION OF ABSTRACT Unclassified	20. LIMITATION OF ABSTRACT UL

THIS PAGE INTENTIONALLY LEFT BLANK

TURBULENCE PROFILES AND OUTER LENGTH SCALE DETERMINATION IN THE ATMOSPHERE USING BALLOONS

Aaron M. Holdaway
Lieutenant, United States Navy
B.S., Harvey Mudd College, 1992

Submitted in partial fulfillment of the
requirements for the degree of

MASTER OF SCIENCE IN PHYSICS

from the

NAVAL POSTGRADUATE SCHOOL
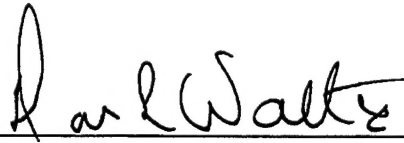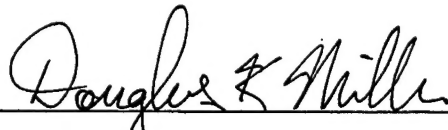March 2000

Author: _____

Aaron M. Holdaway

Approved by: _____

Donald L. Walters, Thesis Advisor

_____

Douglas K. Miller, Co-Advisor

_____

William B. Maier, Chair
Department of Physics

iii

THIS PAGE INTENTIONALLY LEFT BLANK

ABSTRACT

Turbulence in the atmosphere drives the formation of temperature inhomogeneities that scatter and diffract propagating electromagnetic waves, adversely affecting laser weapons and high-resolution optical systems. Military operations require reliable turbulence profiles for the development and validation of turbulence prediction models.

This research investigated the false turbulence contribution caused by well-known temperature steps in the vertical profile of the atmosphere, especially in the stratosphere. The homogeneity and isotropy requirements of structure functions were used to develop a technique to remove the false contribution to the temperature structure constant, C_T^2.

Both 1.54 cm and 5.82 m vertical resolution profiles with 0.001 to 0.01 K temperature resolution were collected from a balloon flight. Steps of 0.1 to 1 K in the vertical temperature profile produce abrupt changes in the mean temperature that obscure the measurement of the actual turbulent fluctuations. Removing these anomalies exposed the underlying C_T^2 distribution. Application of the new technique for several sampling intervals revealed a Kolmogorov inertial subrange extending from ~25 cm to ~10 m. The potential of this technique to compute the isoplanatic angle, θ_0, coherence length, r_0, and Greenwood frequency, f_g, reliably by using inexpensive balloons should benefit airborne and space-based laser programs.

THIS PAGE INTENTIONALLY LEFT BLANK

TABLE OF CONTENTS

THIS PAGE INTENTIONALLY LEFT BLANK

LIST OF SYMBOLS

a_l, a_u — Intercepts of a linear equation

b_l, b_u — Slopes of a linear equation

B — Slope difference, equal to $b_u - b_l$

B_{max} — Maximum desired value for B

B_T — Correlation function of temperature

$C_n^{\,2}$ — Index of refraction structure constant

$C^{(n)}_n{}^{2}$ — Index of refraction structure constant of order n

$C_T^{\,2}$ — Temperature structure constant

$C^{(n)}_T{}^{2}$ — Temperature structure constant of order n

d — Adaptive optics system sub-aperture size

dB — Decibel

D — Aperture diameter

$D^{(n)}_n$ — Index of refraction structure function of order n

$D^{(n)}_T$ — Temperature structure function of order n

f_g — Greenwood frequency

k — Wavenumber of light

L — Propagation path length

l_0 — Inner length scale

L_0 — Outer length scale

m — Power law exponent

n — Index of refraction

N — Noise signal

N_0, N_1, N_2 — Noise signal at heights 0, 1, and 2

P — Pressure

Q — Ratio of step term to turbulent term

Q_{max} — Maximum desired value for Q

r — Sampling interval

r_0 — Coherence length, or Fried parameter

t — Time

T — Temperature

T_0, T_1, T_2 — Temperature at heights 0, 1, and 2

$v_\perp$ — Perpendicular wind component

$W(\omega)$ — Power spectral density

z — Height coordinate

ACKNOWLEDGMENTS

THIS PAGE INTENTIONALLY LEFT BLANK

I. INTRODUCTION

Atmospheric turbulence degrades propagating electromagnetic waves by the processes of scattering and diffraction. Many laser and telescope systems of interest to the military operate within the visible through near infrared portion of the spectrum, referred to as the optical spectrum. Systems that require less than 1-10 μ rad angular resolution are especially prone to degradation from atmospheric turbulence over paths of ~1 km or greater.

The Airborne Laser (ABL), sponsored by the USAF, is a system that transmits a high-energy beam over several hundred kilometers and focuses it to a small spot size. The effects of atmospheric turbulence are a primary limitation to the system performance. Measuring the distortion of the wavefront in near real time and compensating with a deformable mirror can increase the energy density to the level needed to destroy a missile during the boost phase.

The ability to forecast the severity of atmospheric turbulence accurately would be of value in mission planning and coordinating real time operations for ABL and other military adaptive optics systems. Developing a reliable forecast model requires accurate validation data for comparison. The potential of inexpensive meteorological balloons to provide accurate turbulence profiles from the temperature profile is enticing.

A VIZ microsonde package launched in March 1995 from Wichita, Kansas, was augmented with two additional microthermal temperature instruments. They provided 1.54 cm and 5.82 m vertical resolution profiles of temperature in addition to the standard

pressure, temperature, humidity, wind speed and wind direction measurements. The weather consisted of dry snow at low altitudes topped by clear air.

There was cross coupling between the VIZ microsonde electronics package and the high-resolution thermocouple electronics at the 1.25 sec sample period that produced anomalous temperature spikes. These were removed by data processing and editing. Blind application of a second-order structure function to the temperature profiles revealed the signature of temperature steps and confirmed the tendency of the stable stratosphere to organize itself into a stepped profile of temperature on all scales. The homogeneity and isotropy requirements of structure functions led to the development of a quantitative measure and procedure to remove the false turbulence caused by the temperature steps. Confirmation of this technique came from the evidence of a Kolmogorov type inertial subrange after removal of the temperature steps. The inertial subrange extended from ~25 cm to ~10 m. This research produced a reference turbulence profile and measurement procedure suitable for validation of forecast models. Horizontally spaced probes are also subject to these same step effects. Further research may show that a correction factor can remove these effects, or that smaller horizontal separations may be necessary. The opportunity exists for ABL and other programs to take advantage of the narrow Kolmogorov window with inexpensive 5 m vertical resolution instruments.

Chapter II presents a background of theory on optical turbulence, structure functions, and optical parameters. The new theory of temperature steps is also presented. The balloon instrumentation and preliminary data processing are discussed in Chapter III.

Results of the investigation are presented in Chapter IV. Finally, concluding remarks are made in Chapter V.

THIS PAGE INTENTIONALLY LEFT BLANK

II.   BACKGROUND

A.   OPTICAL TURBULENCE

Variations in the index of refraction of a medium distort the wavefront of propagating electromagnetic waves. Consequently, the constant phase surface of the wave departs from a flat surface. Figure 1 shows an incident plane wave passing through a region of fluctuating, optically turbulent, refractive index. The wavefront speeds up/slows down through lower/higher index of refraction regions.

Treating the atmosphere as an ideal gas, the index of refraction, n, becomes a function of pressure P, temperature T, and humidity Q,

$$n = n(P,T,Q) . \tag{1}$$

For air, there is also a weak dependence on wavelength, which is negligible over the optical spectrum (Jones, 1981). For optical wavelengths, the index of refraction may be written as (Tatarski, 1961, pp. 55)

$$n = 1 + \frac{79 \times 10^{-6}}{T} P . \tag{2}$$

Fluctuations in P (mbar) and T (K) from the mean values will result in corresponding fluctuations in the index of refraction. The incremental change in the index of refraction can be found by taking the total differential of n,

$$dn = 79 \times 10^{-6} \left(\frac{1}{T} dP - \frac{P}{T^2} dT \right), \tag{3}$$
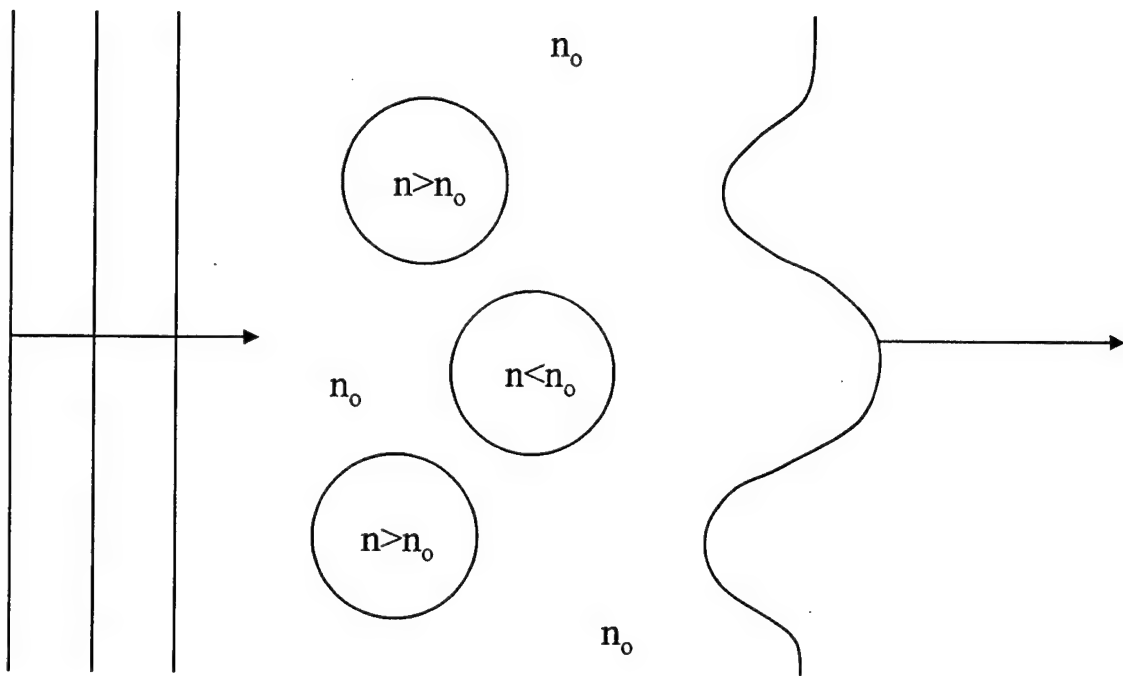
Figure 1. Variations in the index of refraction distort a plane wave as it passes through an optically turbulent medium.

where the two increments represent turbulent departures from the mean. The humidity contribution to Equation (2), not shown, has a negligible contribution to Equation (3) and was ignored for simplicity. A further simplification arises because the pressure variation term is very small compared to the temperature variation term. This is because typical atmospheric wind velocities are small compared to the speed of sound, allowing time for equilibration, which suppresses the formation of acoustic waves.

Positive and negative changes, dn, from the mean index of refraction distort the phase of a propagating wave. By squaring a simplified form of Equation (3), we form a statistical quantity,

$$dn^2 \cong \left(79 \times 10^{-6} \frac{P}{T^2}\right)^2 dT^2, \tag{4}$$

which is closely related to the variance of the fluctuations. The theory of random functions is appropriate in studying the spatially or temporally averaged temperature term, $\langle dT^2 \rangle$, and is discussed in the next section.

B.   STRUCTURE FUNCTIONS

1.   First Order

The variance of a stationary variable, such as temperature, can be written as

$$\langle dT^2 \rangle = \left\langle \left(T - \langle T \rangle\right)^2 \right\rangle. \tag{5}$$

One difficulty with this approach is that the average temperature may vary over the region of interest or over time; it is not stationary. When this occurs, the variance

includes a contribution from the overall change in mean temperature and no longer represents only temperature fluctuations.

Structure functions provide a more robust method to examine the temperature fluctuations than the variance. The 1st order temperature structure function is a function of the temperature at two positions, 1 and 2, and is written as

$$D^{(1)}_T = \left\langle (T_2 - T_1)^2 \right\rangle, \tag{6}$$

where the superscript indicates the function is a first order difference. It quantifies the level of temperature fluctuations without requiring stationarity. The difference completely rejects constant values in the variable, as does the variance in Equation (5). The advantage of the structure function in Equation (6) over the variance is that it rejects gradual shifts in the mean value of temperature common to both terms. As the separation between T_2 and T_1 increases, the difference in the mean values of T_2 and T_1 approaches and eventually dominates the random fluctuations in temperature. At this distance and beyond, the structure function no longer rejects mean value gradients. The steeper the gradient in the mean value, the shorter the separation distance over which the structure function is useful. Higher order structure functions provide a solution to the mean gradient problem and are discussed in Section 2.

Within regions of limited size, when the turbulence is homogeneous and isotropic the structure function of the atmosphere has a Kolmogorov dependence on distance r between the points, 1 and 2, given by (Tatarski, 1961, pp. 46)

$$D^{(1)}_T(r) = C_T^2 r^{2/3}. \tag{7}$$

Since this function increases with separation distance, it is interpreted as a measure of the temperature turbulence. For homogeneous turbulence, the structure function is related to the correlation function in the following manner,

$$D^{(1)}_T(r) = 2[B_T(0) - B_T(r)],$$ (8)

where $B_T(r)$ is the correlation function of temperature (Tatarski, 1961, pp. 10). Equation (8) provides additional insight into why structure functions begin at zero and rise with r monotonically.

The index of refraction structure function has the same form as the temperature structure function in Equation (7),

$$D^{(1)}_n(r) = C_n^2 r^{2/3},$$ (9)

where the index of refraction structure constant is related to the temperature structure constant by, refer to Equation (4), (Tatarski, 1961, pp. 79)

$$C_n^2 = C_T^2 \left(79 \times 10^{-6} \frac{P}{T^2} \right)^2.$$ (10)

2.   Higher Order

Generalized structure functions of nth order have the advantage that they remove polynomial trends in the data of order n-1. This property makes them useful in analyzing geophysical variables such as temperature and wind speed. For example, a second-order structure function removes both a constant and a linear trend in the data. The second-order structure function uses the difference in the slopes of the temperature profile at two

9

points, A and B. The slopes at A and B are found from a finite difference in the temperature,

$$\left(\frac{dT}{dz}\right)_B \propto T_2 - T_1, \qquad\qquad \left(\frac{dT}{dz}\right)_A \propto T_1 - T_0. \tag{11}$$

The second-order structure function becomes

$$D^{(2)}{}_T = \left\langle \left[(T_2 - T_1) - (T_1 - T_0) \right]^2 \right\rangle = \left\langle \left[T_2 - 2T_1 + T_0 \right]^2 \right\rangle. \tag{12}$$

In general, the nth order structure function (Yaglom, 1987, pp. 427) can be written in terms of the function at $n+1$ different points and the binomial coefficient,

$$D^{(n)}{}_T = \left\langle \left[\sum_{k=0}^{n} (-1)^k \binom{n}{k} T_k \right]^2 \right\rangle. \tag{13}$$

The theory has an interesting and useful result for structure functions of the form

$$D^{(n)}{}_T(r) = C^{(n)}{}_T{}^2 r^m, \tag{14}$$

under which the Kolmogorov expression in Equation (7) falls. For $m > 0$, the various order coefficients obey the relation,

$$C^{(n)}{}_T{}^2 = C^{(1)}{}_T{}^2 \sum_{j=0}^{n-1} \binom{2n}{j} (-1)^{n+j} (n-j)^m, \tag{15}$$

to the first order coefficient (Walters, 1995). The 1$^{\text{st}}$ order coefficient is the desired quantity, with $C_T{}^2 = C^{(1)}{}_T{}^2$, and is found in Chapter IV from the 2$^{\text{nd}}$ order structure

function by the ratio $C_T{}^2 = C^{(2)}{}_T{}^2 / 2.412$. Section D will show the utility of the temperature and index of refraction constants.

3.   Inertial Subrange and Power Spectrum

This section discusses the limits and behavior of the Kolmogorov result in Equation (7). The Kolmogorov structure function behavior holds for homogeneous and isotropic volumes. Beyond the outer scale length, L_0, the assumptions do not hold and the law fails. For example, the turbulence in a thundercloud is quite different from the quiescent air just outside the boundary of the cloud, introducing anisotropy. As the turbulent cascade proceeds to smaller eddies, the viscous dissipation of the air increases and ideally prevents turbulent motion below an inner length scale, l_0, having converted the turbulent kinetic energy of motion into thermal energy of the air molecules. Using a power series expansion, the structure function has an r^2 power law below l_0 (Tatarski, 1961, pp. 32). Figure 2 illustrates the idealized behavior of experimentally determined temperature structure functions against the theoretical functions.

The power spectrum of a turbulent variable reveals the range over which the Kolmogorov power law applies. Figure 3 is a representative log-log plot of an idealized one-dimensional temperature power spectrum. The inertial subrange is the region with constant slope, where the $-5/3$ slope follows from the $r^{2/3}$ form of the structure function law (Tatarski, 1961, pp. 25). This result hails from the general equation relating the structure function of Equation (14) to the power spectral density $W(\omega)$,
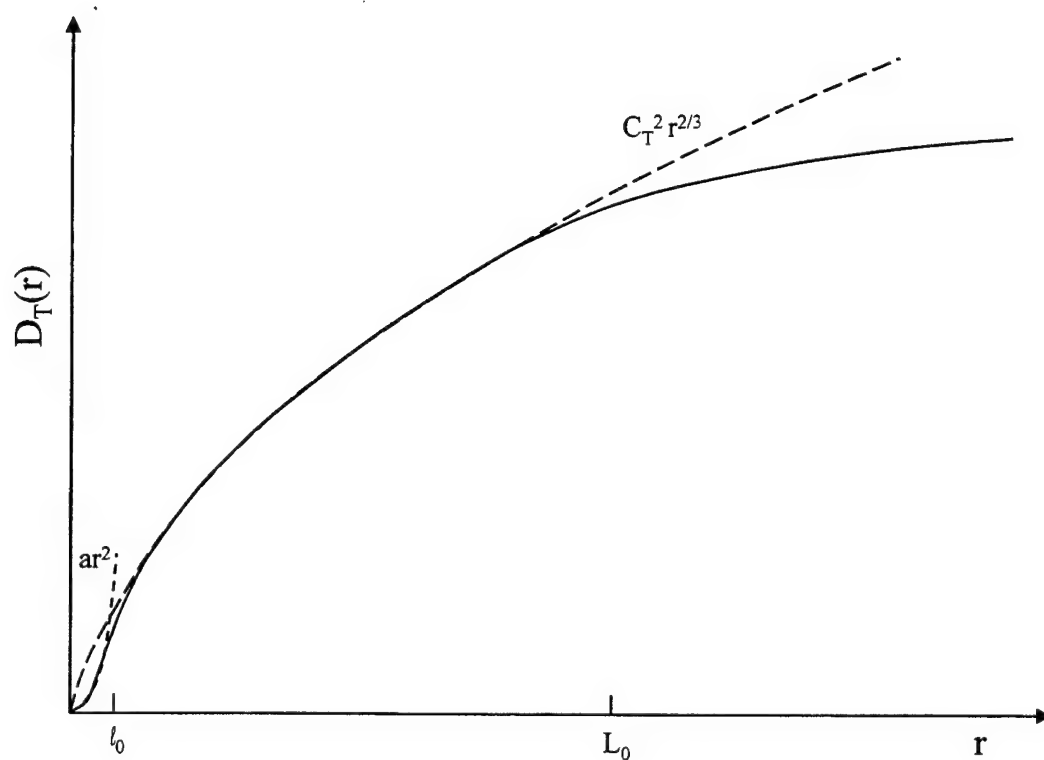
Figure 2. Idealized structure function behavior with sampling interval r. The Kolmogorov 2/3 law holds between l_0 and L_0. Quadratic behavior is observed below l_0. After Tatarski, 1961, pp. 33.
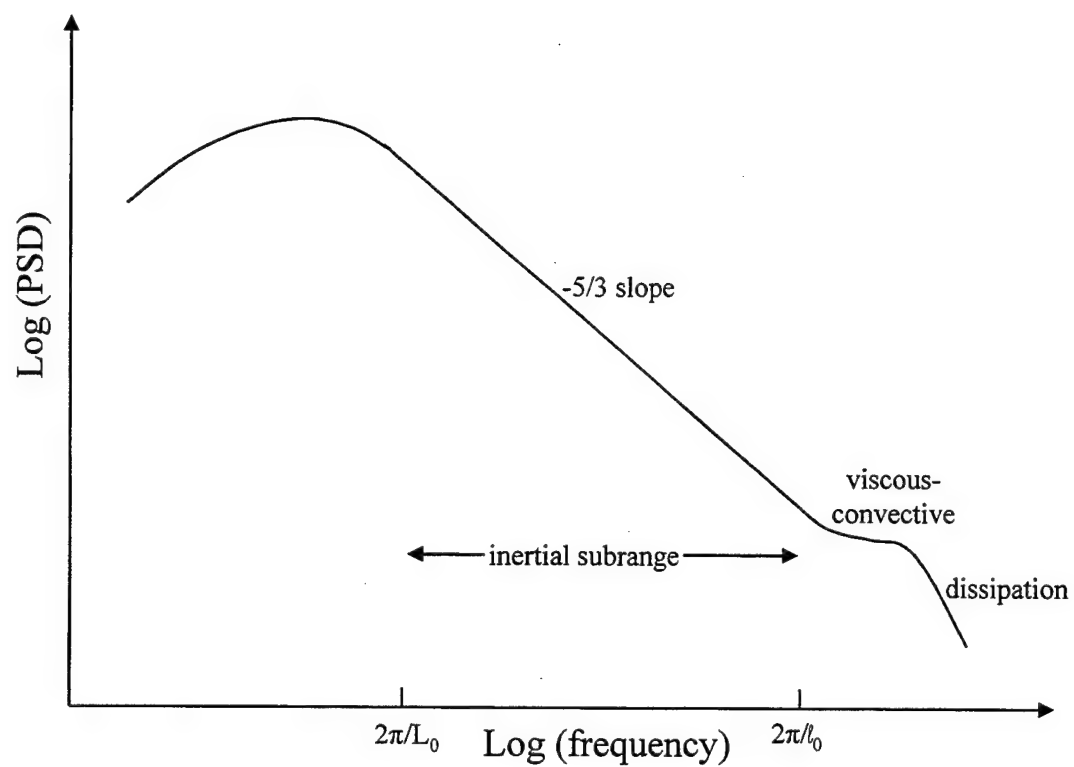
Figure 3. Idealized power spectrum of temperature as a function of frequency. The inertial subrange, viscous-convective, and dissipation regions are shown (Tennekes, 19, pp. 284).

$$W(\omega) = \frac{\Gamma(1+m)}{2\pi} \sin \frac{\pi m}{2} C_T{}^2 |\omega|^{-(m+1)}, \tag{16}$$

for $0 < m < 2$ (Tatarski, 1961, pp. 13). Inner and outer scale lengths are obtained from the spatial frequencies that bound the power law region of the spectrum. The dissipation, or viscous convective, kink at the right end of the spectrum is a result of the mechanical viscosity stopping the turbulent motion before temperature diffusion can equalize the temperature. Beyond the kink, the spectrum falls off rapidly as thermal diffusion smoothes the variations.

C.   TEMPERATURE STEPS

The structure function approach can fail when applied over a region that is not homogeneous and isotropic. A false contribution to the second-order structure function can occur when the gradient of the temperature profile changes appreciably over the measurement distance with respect to the fluctuations. Figure 4 presents a simple model in which the temperature increases with slope b_l below, and slope b_u above, height z_1. The abrupt change in slope alters the behavior of the structure function.

Consider the temperature, $T(z,t)$, as a function of height, z, and time, t,

$$T(z,t) = \bar{T}(z) + \xi(z,t), \tag{17}$$

to be a sum of the mean, time averaged, temperature, $\langle T(z,t) \rangle_t = \bar{T}(z)$, and a fluctuation term, $\xi(z,t)$, representing the turbulence. By this definition, the time average of the fluctuation term is zero,
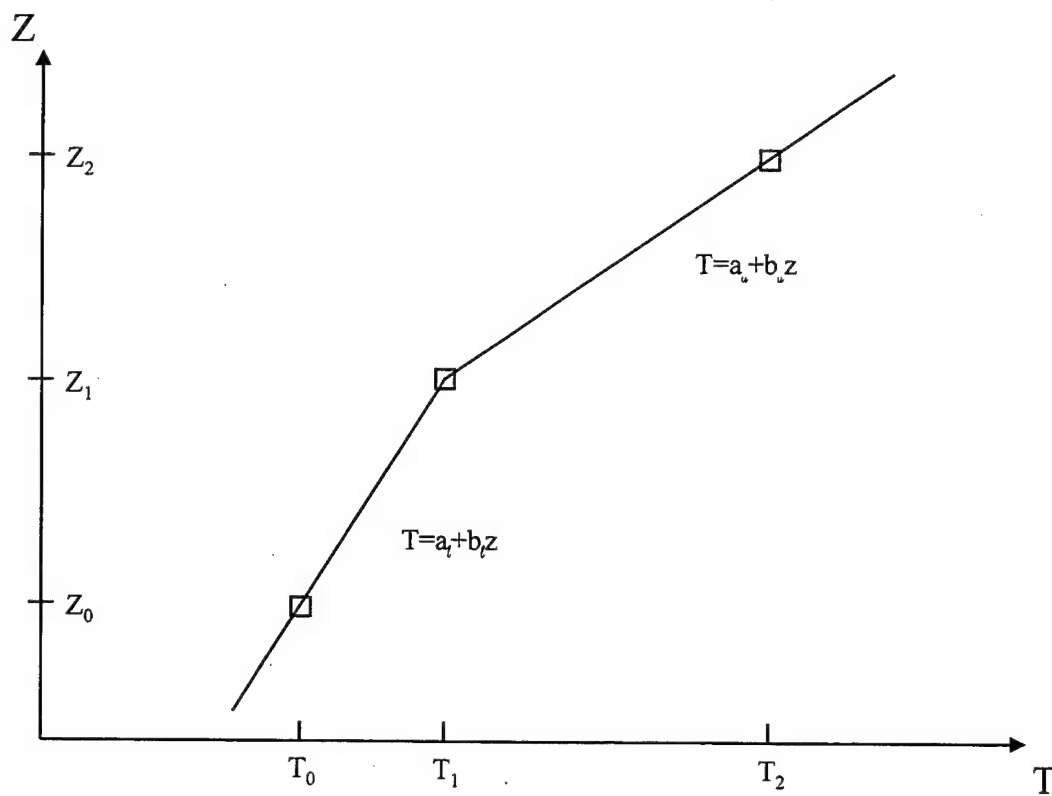
14

Figure 4. A simple model of a temperature step. Second-order structure functions computed at the step, slope discontinuity, are artificially high.

$$\langle \xi(z,t) \rangle_t = 0.$$ (18)

Following Figure 4, the linear function of temperature with height is

$$\overline{T}(z) = \begin{cases} a_u + b_u z, & z \geq z_1 \\ a_l + b_l z, & z \leq z_1 \end{cases},$$ (19)

where a_u, a_l, b_u, and b_l are constants. Continuity of temperature across the step results in the boundary condition,

$$a_l + b_l z_1 = a_u + b_u z_1.$$ (20)

Substituting the expressions for temperature in Equation (19) into the second-order structure function of Equation (12) yields

$$D^{(2)}{}_T(r) = \left\langle [T_2 - 2T_1 + T_0]^2 \right\rangle = \left\langle [(b_u - b_l)r + (\xi_2 - 2\xi_1 + \xi_0)]^2 \right\rangle.$$ (21)

The difference operation eliminates the constants, a_u and a_l, and the sampling interval $r = z_2 - z_1 = z_1 - z_0 = \Delta z$ is the height increment. Equation (21) now includes terms for the slopes and the temperature fluctuations. Rewriting $B = b_u - b_l$ and multiplying out the terms results in,

$$D^{(2)}{}_T(r) = \left\langle [Br]^2 \right\rangle + \left\langle [(\xi_2 - 2\xi_1 + \xi_0)]^2 \right\rangle,$$ (22)

after using Equation (18) to eliminate the cross terms. The second term of Equation (22) is the desired 2nd order structure function. Using the Kolmogorov expression in Equation (7) and the ratio $C_T{}^2 = C^{(2)}{}_T{}^2 / 2.412$, from Equation (15), gives

16

$$D^{(2)}{}_T(r) = B^2 r^2 + 2.41 C_T{}^2 r^{2/3}. \tag{23}$$

The measured 2nd order structure function is a combination of the true temperature turbulence, obeying a 2/3 law, and a false quadratic slope discontinuity term. A measure of the relative contribution by the slope discontinuity term is the ratio

$$Q = \frac{B^2}{2.41 C_T{}^2} r^{4/3}. \tag{24}$$

The second-order structure function must only be calculated within constant gradient or homogenous regions under isotropic conditions in order to preclude a false contribution.

Removing the steps from the structure function should reveal the true turbulence constant, $C_T{}^2$. Although the development pertains to 2nd order structure functions, the theory is general to nth order. Slow trends in the mean value may be ignored with 1st order structure functions if the corresponding Q factor is much smaller than 1, as was mentioned in Section B. Similarly, rapid changes in curvature would add a false contribution to 3rd order structure functions, etc.

D.   OPTICAL PARAMETERS

1.   Coherence Length

The coherence length, r_0, or Fried parameter, is useful because it is the equivalent maximum aperture an optical system could have and still obtain a near perfect diffraction limited image, $\varphi_{res} = \lambda / r_0$ vice $\varphi_{res} = \lambda / D$. Equivalently, the maximum sub-aperture size of an adaptive optics system, d, is dictated by the lowest value of r_0 for which it is

necessary to compensate. Physically, it is a characteristic scale over which the electromagnetic field has approximately constant phase. For a plane wave,

$$r_0 = 2.1\left(\frac{2.91}{2}k^2\int_0^L C_n^{\,2}(z)dz\right)^{-3/5},$$ (25)

where the integral is of the phase fluctuations that accumulate along the propagation path, z, k is the wavenumber, and $C_n^{\,2}(z)$ characterizes the magnitude of the optical turbulence (Fried, 1966). We now see the utility of the structure function approach in providing a robust parameter that can be used to characterize the atmospheric turbulence.

2.   Isoplanatic Angle

Adaptive optical systems function by correcting the distorted wavefront based upon a measurement of the phase of the electromagnetic field. Since atmospheric turbulence varies with position, the correction for a specific source along an optical path, such as a star, is path dependent. The isoplanatic angle,

$$\theta_0 = \left(2.91k^2\int_0^L C_n^{\,2}(z)z^{5/3}dz\right)^{-3/5},$$ (26)

is a measure of the angular separation between two sources for which the accumulated phase distortions are correlated (Fried, 1982). It is the angle where the Strehl ratio of an ideal adaptive optics system drops to e^{-1} of perfect performance. The Strehl ratio is the ratio of actual peak intensity to the diffraction limited peak intensity. Isoplanatic angle is calculated by a vertical integration through the atmosphere weighted by the height, and is

basically the spherical path coherence length divided by the path length, $\theta_0 \approx r_0 / L$. The weighting occurs because two points higher in the atmosphere are farther apart and accumulate larger phase differences between the two propagation paths.

3.   Greenwood Frequency

Wind advects the turbulent air across the optical path, changing the turbulent fluctuations. The Greenwood frequency,

$$f_g = \left(0.1024 k^2 \int_0^L C_n^2(z) v_\perp^{5/3}(z) dz \right)^{-3/5}, \tag{27}$$

is found by integration over the optical path, taking into account the displacement caused by the wind component, $v_\perp$, perpendicular to the integration path (Greenwood, 1977). It is a measure of the sampling rate an adaptive optics system must have to compensate for the turbulent degradation. Typically, an adaptive optics system with a bandwidth of $4 f_g$ will have a 3 dB loss in Strehl ratio.

THIS PAGE INTENTIONALLY LEFT BLANK

III. IMPLEMENTATION

A. BALLOON FLIGHT

A meteorological balloon sounding was taken at 0700 UT on 5 March 1995 from Wichita, Kansas, to measure the vertical temperature profile with high resolution (D. L. Walters, NPS). High-resolution and medium-resolution temperature instruments were added to the standard VIZ balloon package, providing 1.54 cm and 5.82 cm vertical resolution temperature profiles, respectively. The theory of structure functions allowed subsequent computation of the optical turbulence profiles.

The weather consisted of light, dry, snow below 2 km, topped by clear air. The balloon ascended through the stratosphere at 4.7 m/s on average, to an altitude of over 19 km. Pressure, temperature, and humidity were recorded every 1.25 seconds, at an average 5.8 m spacing. Height above ground was determined from the hypsometric equation (Holton, 1979, pp. 19). Wind speed and direction were recorded every 30 seconds.

The standard VIZ low-resolution temperature probe had a time constant of about 30 seconds and was sampled every 1.25 seconds. A medium-resolution, 100 μm bead thermistor added to a spare channel in the VIZ package provided more detailed temperature features of the atmosphere. The time constant increased with decreasing atmospheric pressure from 30 msec at ground level to 100 msec at 15 km. Hardware

limitations in the VIZ package limited the sampling interval to 1.25 sec. The temperature resolution of the micro-bead thermistor was between 0.005 and 0.01 K. (Fuehrer, 1994)

Figure 5 shows the low-resolution and medium-resolution temperature profiles. The mismatch was caused by a non-linearity in the medium-resolution probe calibration, resulting in a negligible ~3% error. There was an inversion layer at 1.2 km and the tropopause was at 9.5 km. Figure 6 shows the medium-resolution potential temperature, which is the Kelvin temperature corrected for a dry adiabatic lapse rate, with 1000 mbar reference. The steep positive slope above the tropopause makes the stratosphere buoyantly stable. Large steps are visible throughout the profile. The wind speed and azimuth are plotted in Figure 7. High winds extended from 6 to 15 km, with strongest wind shear at the top boundary.

B.   HIGH RESOLUTION INSTRUMENT

1.   Description

The high-resolution temperature probe was a $12.4 \mu m$ chromel-constantan thermocouple, sampled approximately 315 times per second. Frequency modulation of the VIZ radio signal allowed the high data rate. This resulted in an average height resolution of 1.54 cm. The time constant of the thermocouple increased with decreasing pressure from 5 msec at ground to 15 msec at 20 km (Roper, 1992, pp. 62). To achieve milli-Kelvin resolution with a 12-bit A/D converter required a means of keeping the temperature in the middle of the dynamic range. This was accomplished by measuring
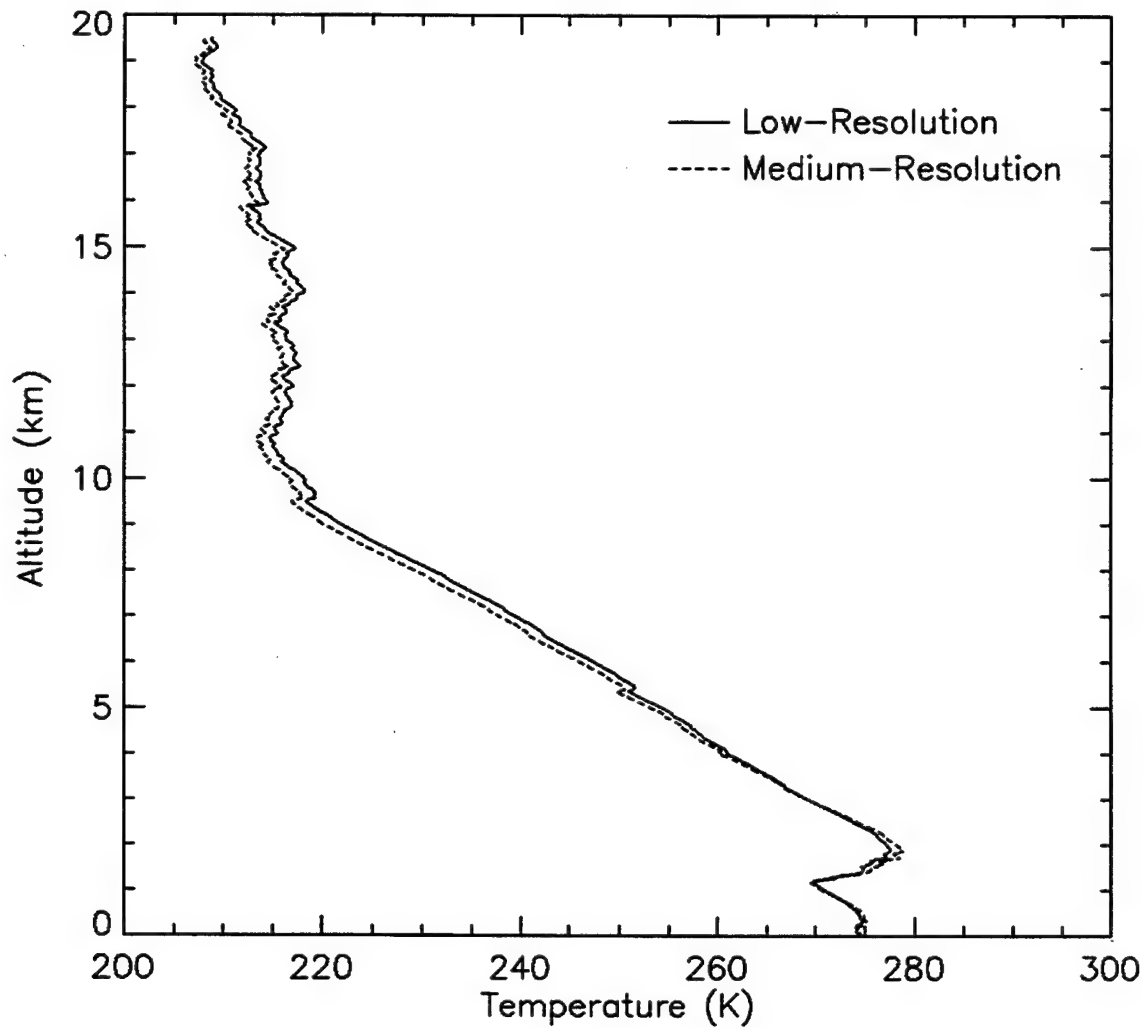
Figure 5. Low-resolution and medium-resolution temperature plotted against altitude. The mismatch between the profiles was caused by altitude non-linearity in the medium-resolution instrument. An inversion layer existed at 1.2 km and the tropopause was at 9.5 km.

23
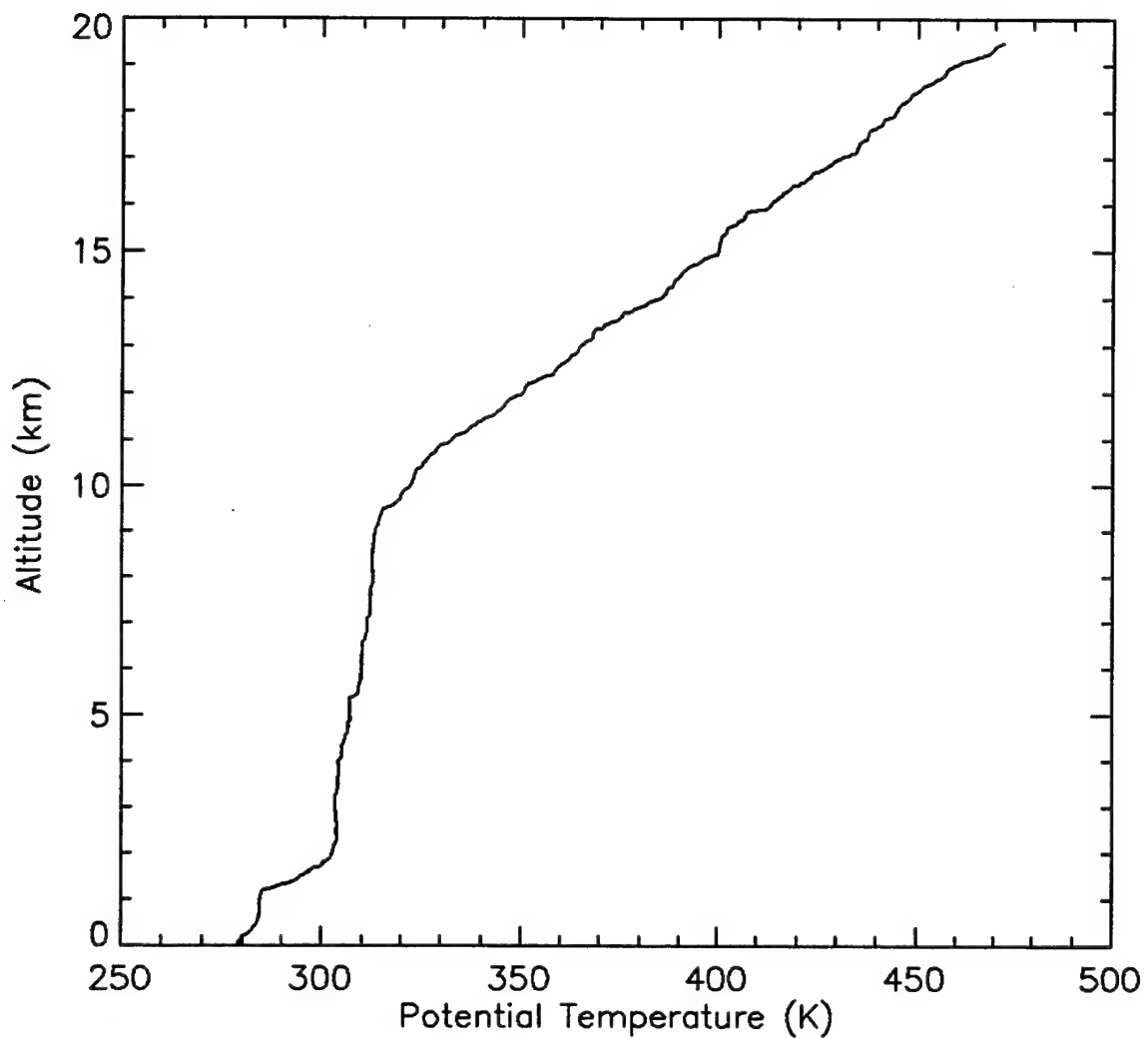
Figure 6. Medium-resolution potential temperature plotted against altitude. The steep slope above 9.5 km makes the stratosphere buoyantly stable. The largest steps are visible throughout the profile. The troposphere was weakly stable, except for the strongly stable inversion layer from 1.2 to 1.9 km.
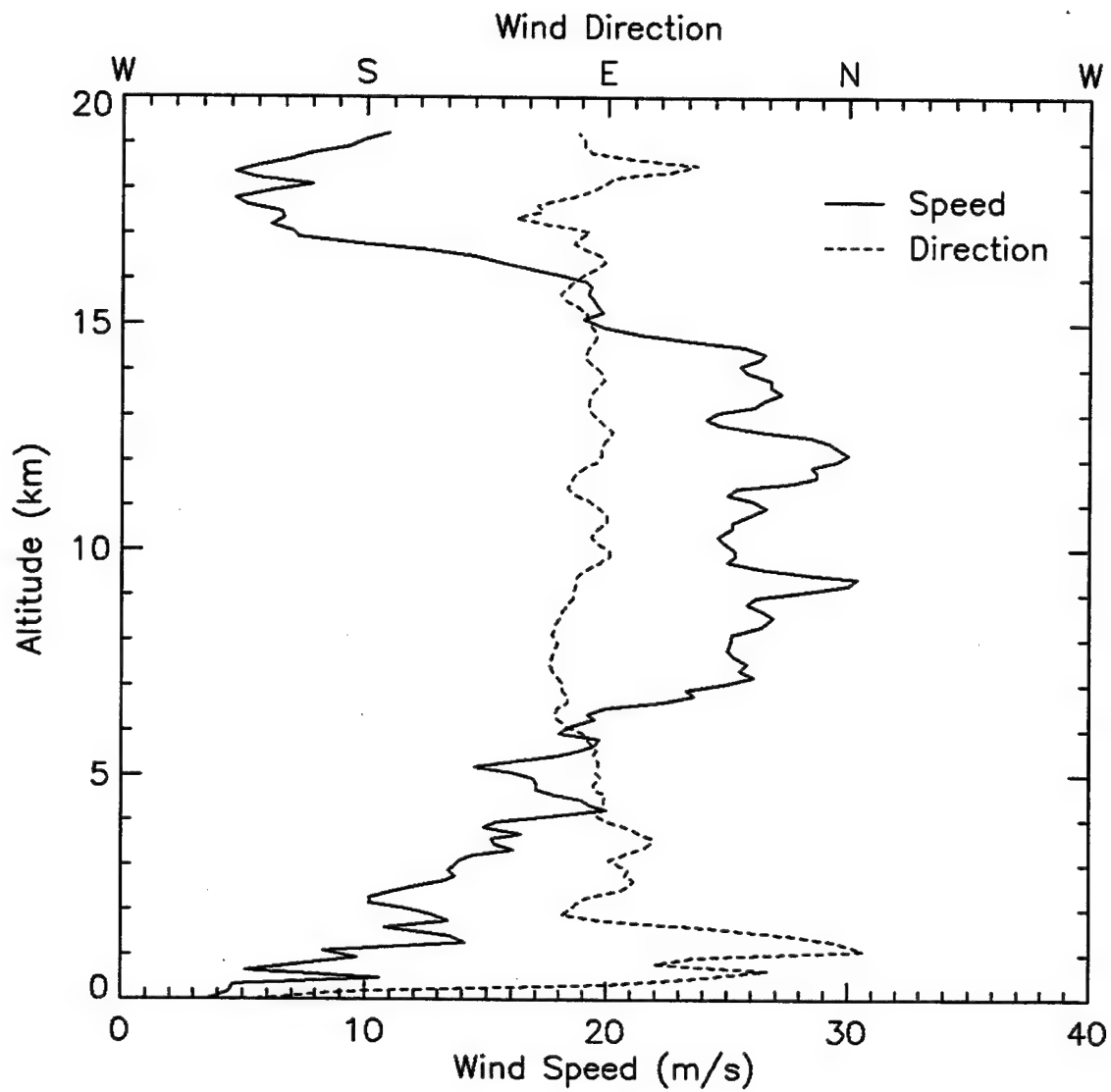
Figure 7. Wind speed and direction plotted with altitude. High winds extended from 6 to 15 km, with strongest wind shear at the top boundary.

the difference between the high-resolution thermocouple and a much slower responding thermocouple, with 10-30 second time constant from ground to 15 km. (Walters, 1995)

Figure 8 shows the high-resolution temperature profile. Data was lost from 1.2 km to 1.9 km because the A/D converter reached full scale in the sharply warming inversion layer. The stratosphere had larger temperature steps than the troposphere. Several regions of large vertical temperature gradient were compared to confirm the conversion from A/D counts to Kelvin. Figure 9 is a plot of high and medium-resolution temperature for one of these regions. Both instruments agreed on the magnitude of the temperature change, confirming absolute calibration of the high-resolution instrument.

2.   Interference Spikes

The 1.25 second interval read-out of low-resolution temperature by the VIZ package induced a signal into the co-located high-resolution cable. The resulting interference spikes are visible in Figure 9, spaced every 6 m, and were characterized by a sudden drop and rise in temperature lasting ~0.1 seconds. The magnitude of the spikes was about 0.02 K with a vertical extent of ~0.5 m.

The effect of the spikes on the measured value of temperature turbulence was quite significant in regions of low turbulence. In a study of six non-turbulent regions throughout the stratosphere, ranging from 65 m to 185 m in vertical extent, a 3 to 10 times increase in the local average C_T^2 due to the spikes was observed. The maximum effect occurred for sampling interval r of 30 cm to 40 cm, which was tuned to the width of the spikes. Significant contamination for sampling intervals of less than 2 m required their removal.

26
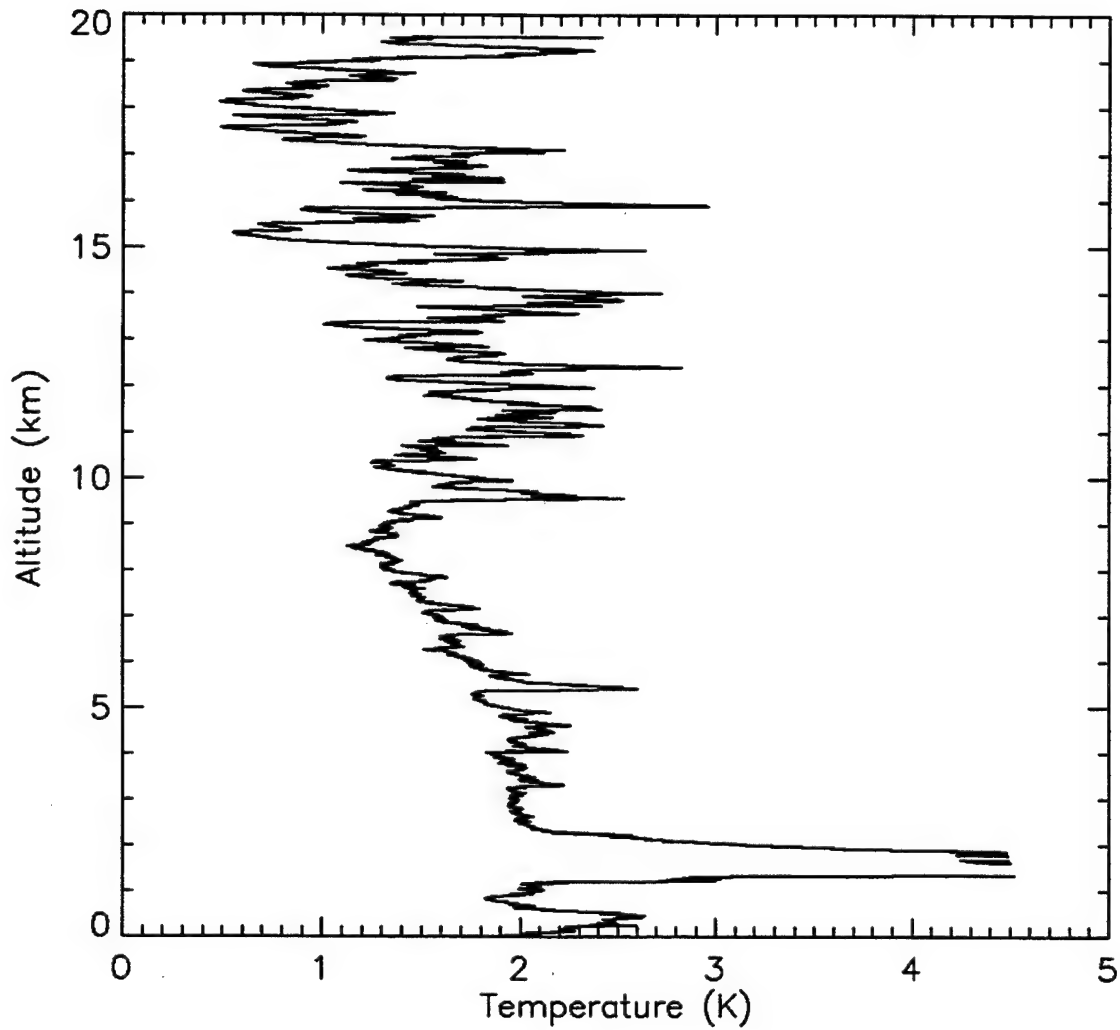
Figure 8. High-resolution temperature plotted against altitude. Data loss occurred from 1.2 km to 1.9 km when the A/D converter reached maximum counts in the inversion layer. The stratosphere had larger temperature steps than the troposphere.

Figure 9. High-resolution temperature and medium-resolution temperature plotted against altitude. This temperature step was used to verify the conversion of high-resolution temperature from counts to Kelvin. The periodic interference spikes in high-resolution temperature are visible at approximately 6 m intervals.

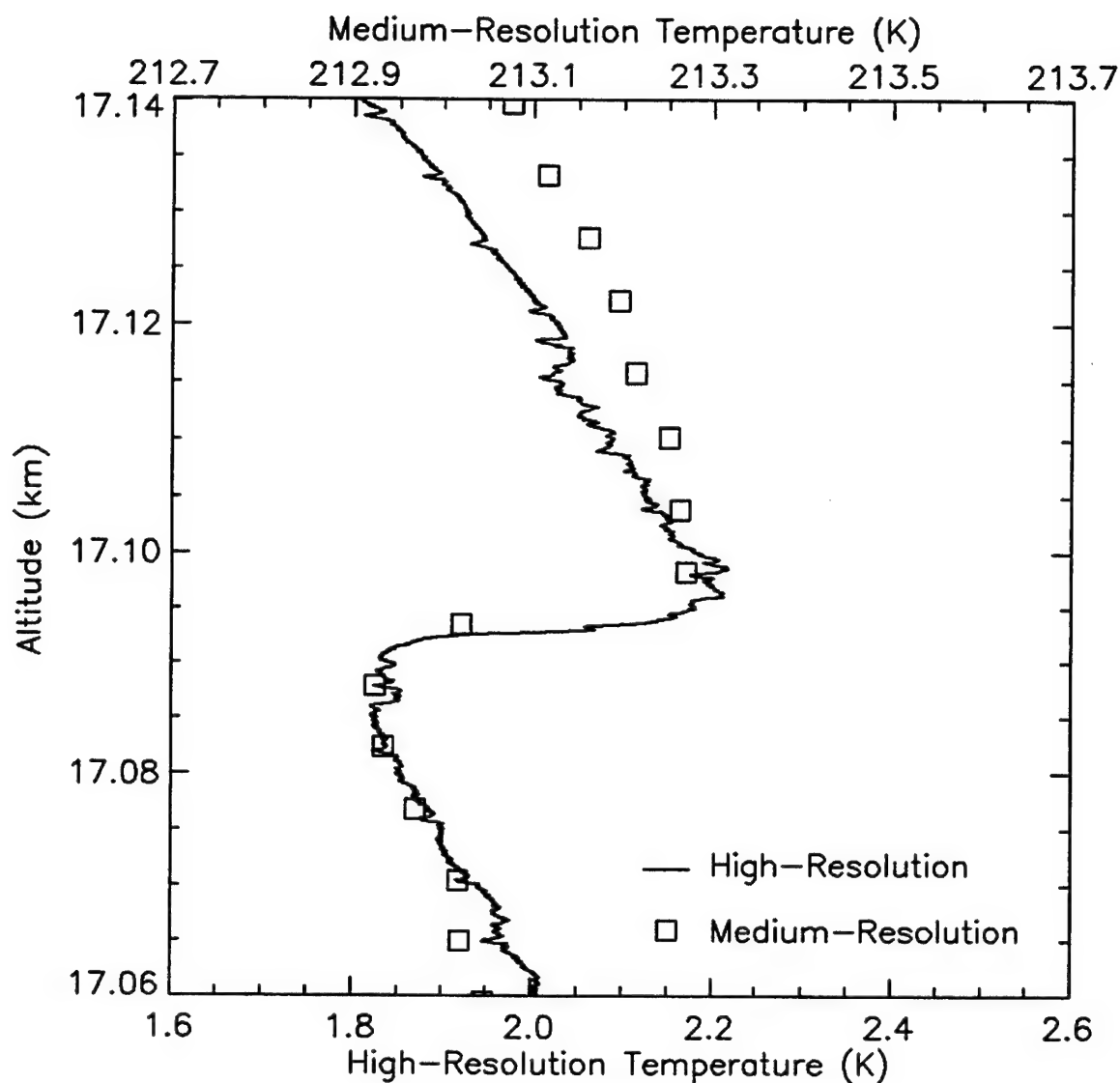The spike contribution to the temperature turbulence was removed by manually viewing the data and flagging the spikes. Numerous regions with turbulent fluctuations ≥ 0.02 K obscured ~27% of the spikes and no attempt was made to remove them. Their contribution was considered negligible if not visually detectable.

Since approximately 7% of the raw high-resolution data were discarded by spike removal, two processing procedures were used to compensate for the missing data. For a given sampling interval, r, four profiles of C_T^2 were generated, each one offset by a quarter of the sampling interval. Subsequent averaging of the four C_T^2 profiles greatly reduced the occurrence of missing data. Figure 10 shows the histogram of the average value of C_T^2 in the stratosphere determined from 0.5 m sampling, where noise suppression was applied to the raw profile per Section 3. The distribution is visually log-normal. Based upon this observation, the remaining missing data were filled in with a local logarithmic average of 11 values. This number was adequate for the smallest r, yet not too large to alter the distribution significantly. Replacing the missing values maintained the approximately log-normal distribution. The procedure narrowed the distribution, reducing the linear average by 11%.

The average value of C_T^2 in the stratosphere was computed for r less than 3 m to investigate the effect of the interference spikes on the stratospheric average. Figure 11 shows that the spikes contributed to the turbulence mainly on length scales below 2 m. This confirmed again that the maximum effect was for 30 cm to 40 cm.
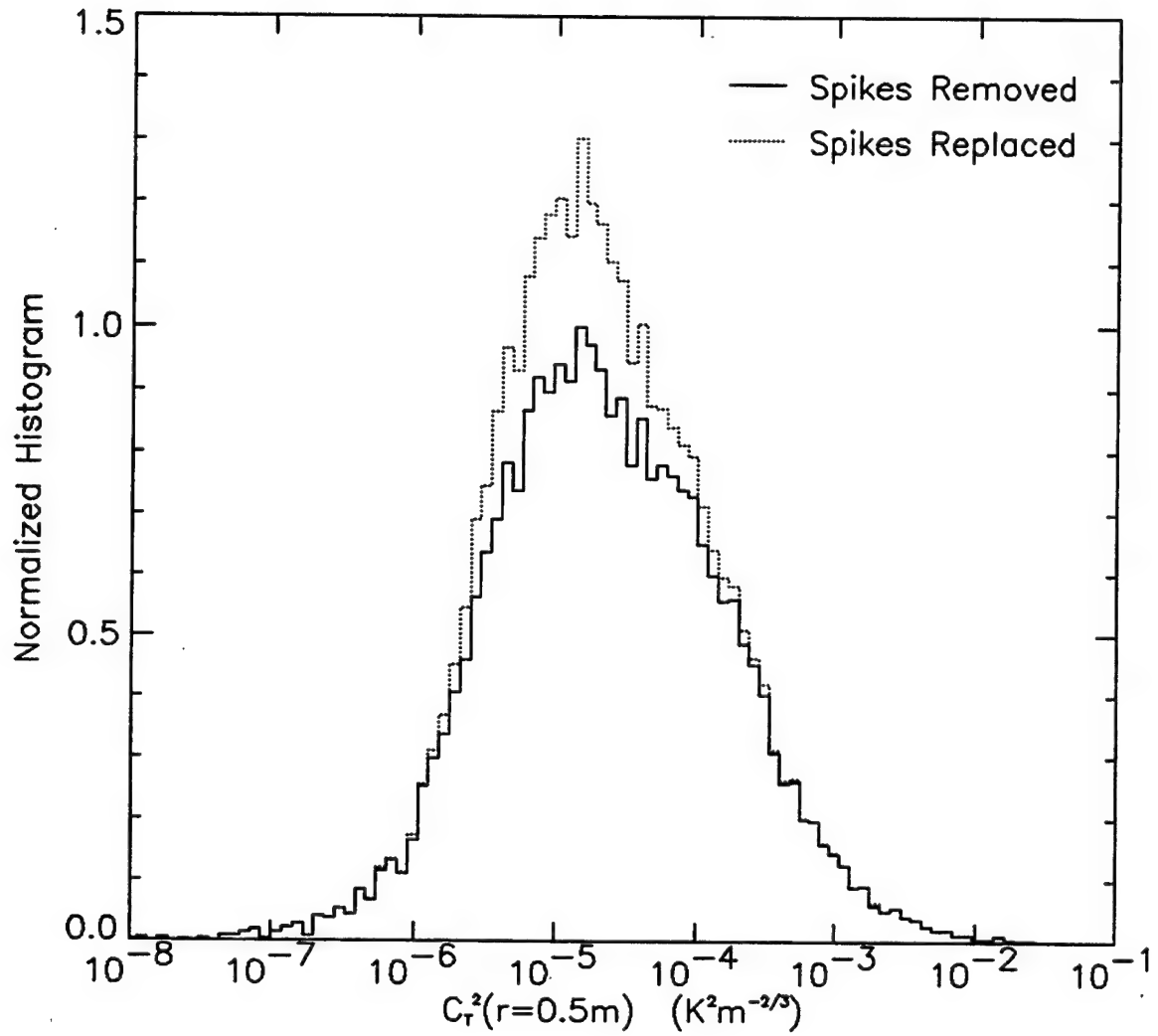
Figure 10. Histogram of the turbulence parameter in the stratosphere using a 0.5 m sampling interval. The effect of replacing data in gaps created by the spike removal is shown. Replacing the interference spike regions with a local logarithmic average narrowed the distribution and reduced the linear average by 11%.

Figure 11. Average turbulence parameter in the stratosphere plotted against sampling interval. Removing the interference spikes and replacing them with a local logarithmic average reduced the contamination, which was primarily below 2 m.

3. Noise Suppression

The power spectral density of the high-resolution temperature in the stratosphere, with linear trend removed, is plotted in Figure 12. The slope of the power spectrum is between -2 and -3, and decidedly steeper than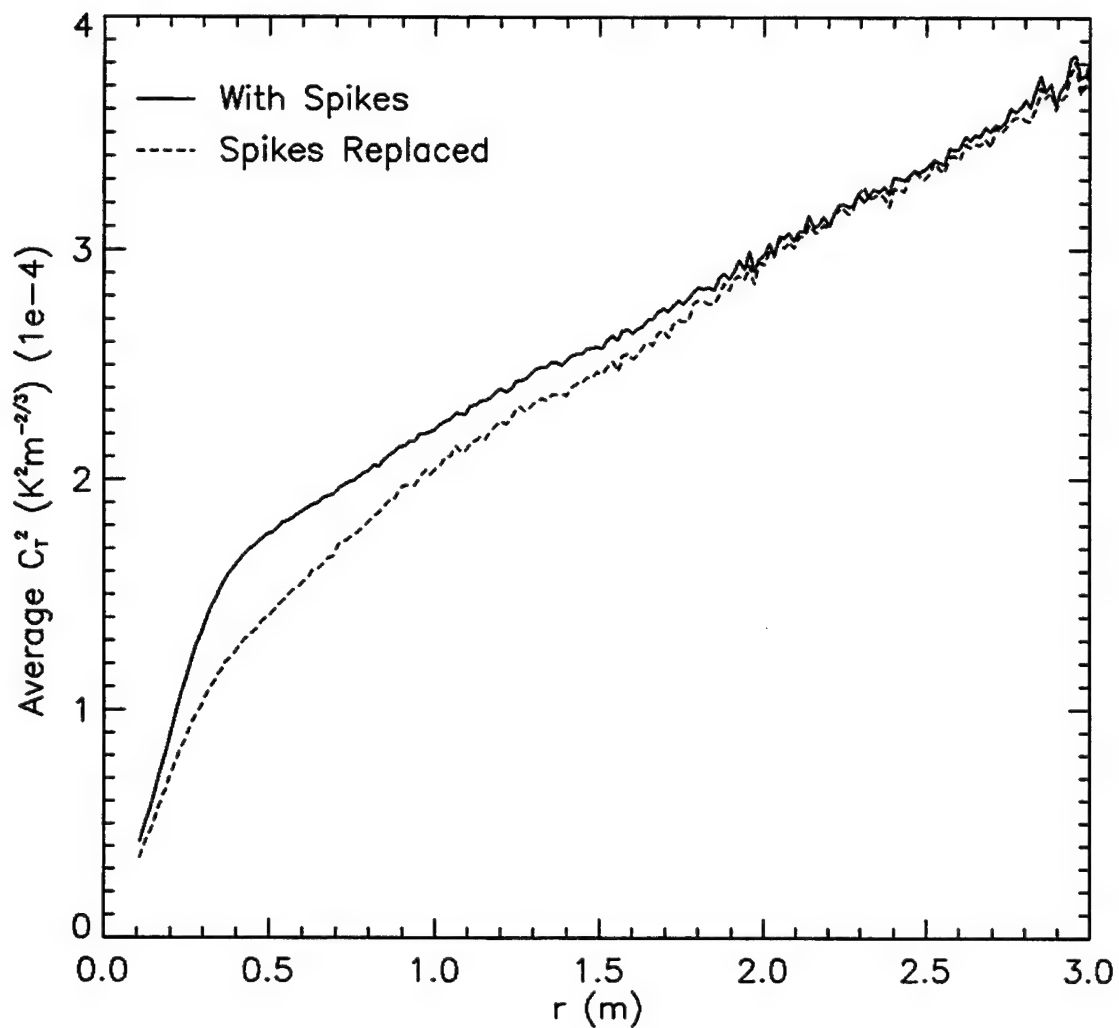 the $-5/3$ Kolmogorov result. The narrow spectral features from 1-10 Hz are harmonics of the 1.25 second period interference spikes. The sensor noise floor dominated above 30 Hz. The thermocouple time constant had a 3 dB cutoff at ~67 Hz, and the 315 Hz sample rate ensured oversampling of the probe. The power rose above 80 Hz from aliasing of the system white noise.

To suppress noise, the raw data set was convolved with a triangular filter. This was equivalent to applying a sinc^2 filter in the frequency domain, with 3 dB point at 45 Hz and first zero at 105 Hz. Noise was greatly reduced with the trade off that the minimum sampling interval, r, was limited to the 6 data point width of the triangle, or 9.24 cm.

The average value of the second-order structure function computed at the raw data resolution served as the noise estimate. Following the theory in Chapter II, Section C, the temperature can be written as a function of height, z, and time, t,

$$T(z,t) = \xi(z,t) + N(z), \tag{28}$$

where $N(z)$ is the noise signal and $\xi(z,t)$ the temperature turbulence. The presence of a slope discontinuity was ignored for simplicity. Assuming the system noise and turbulent fluctuation terms were independent leads to an equation similar to Equation (22),

$$D^{(2)}{}_T(r) = \left\langle [N_2 - 2N_1 + N_0]^2 \right\rangle + \left\langle [\xi_2 - 2\xi_1 + \xi_0]^2 \right\rangle. \tag{29}$$
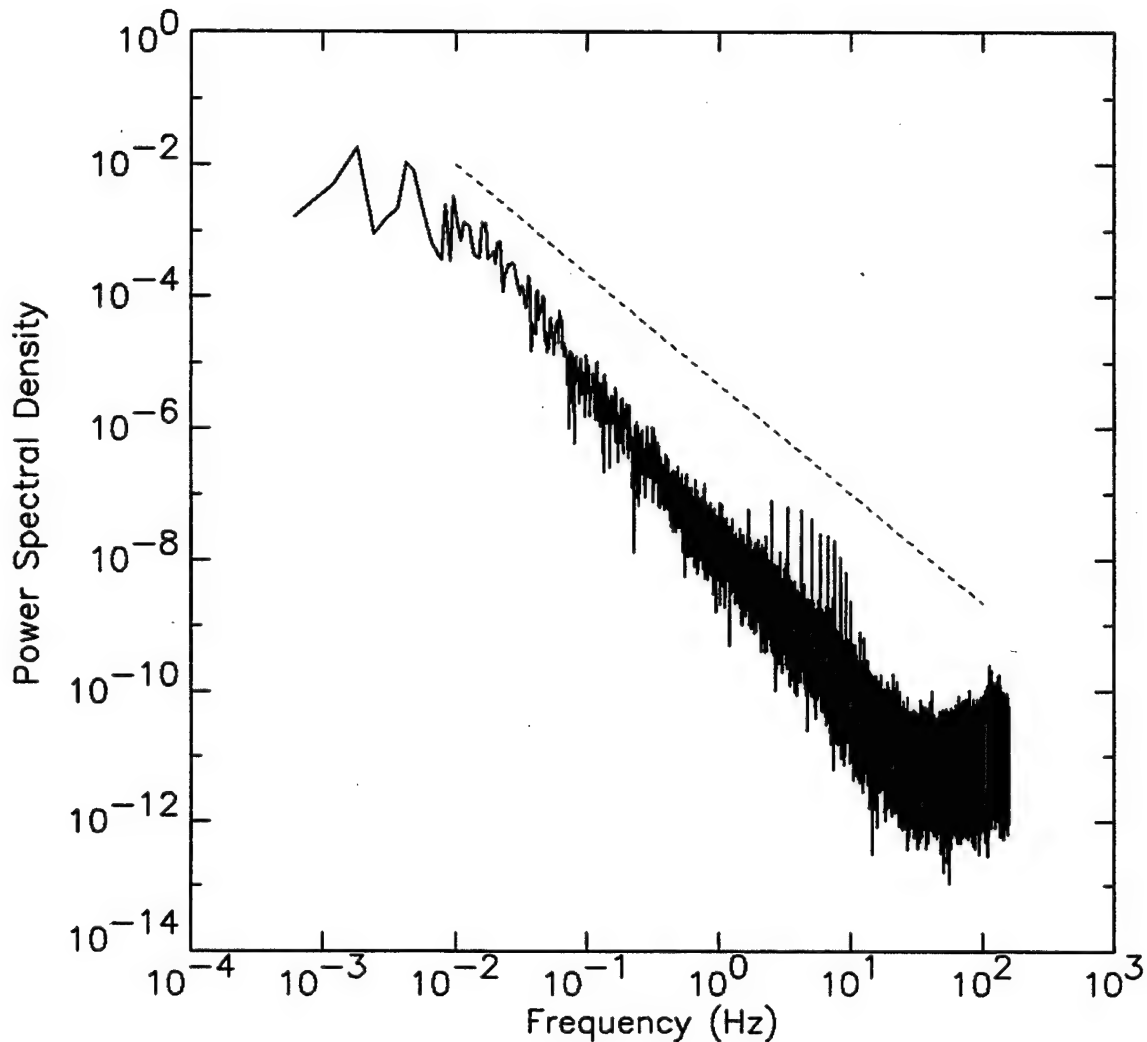
Figure 12. Power spectral density of the stratosphere plotted against frequency. The power spectrum was steeper than the –5/3 Kolmogorov theory, shown with the dashed line. The distinct features from 1-10 Hz are harmonics of the 1.25 second period interference spikes. The noise floor dominated above 30 Hz and the power rose above 80 Hz from aliasing of under-resolved system noise.

The noise is independent of the sampling interval, r, and so may be used for all r once determined. Because of the high-resolution instrument's time constant, it was assumed that negligible real turbulent signal existed at the 315 Hz sampling rate. The value of the second-order structure function at 315 Hz was thus used as the noise estimate for all r.

IV. RESULTS

A. TEMPERATURE STEP EFFECTS

Temperature steps, or slope discontinuities, were abundant in the high-resolution temperature profile, recall the example in Figure 9. They also occur at the boundaries of "sheets" that have been observed by others, (Bertin, 1997), (Dalaudier, 1994), and mechanisms of their formation have been proposed (Coulman, 1995). Equation (22) in Chapter II describes their contribution to the second-order structure function, $D^{(2)}_T(r)$. The temperature structure constant, $C_T{}^2$, increased with sampling interval, r, see Figure 11. This result confirmed that the Kolmogorov relationship for the structure function in Equation (7) failed for this data set. The positive slope of $C_T{}^2$ versus r also indicates a power law with exponent greater than 2/3.

Figure 13 shows the second-order structure function, $D^{(2)}_T(r)$, calculated by averaging the entire stratosphere, where noise suppression and spike removal were performed per Chapter III. Both the high-resolution and medium-resolution data are plotted. Beyond 100 m, the A/D converter high-pass difference filter reduced the high-resolution signal. The Kolmogorov 2/3 slope and the step-removed values are plotted for reference and are further discussed in Section 2.

The power law exponent, $m(r)$, of $D^{(2)}_T(r)$ is plotted in Figure 14. The high-resolution and medium-resolution instruments agreed well below 100 m, the maximum useful value of the high-resolution instrument. The rise in slope towards 2 for small r is

35
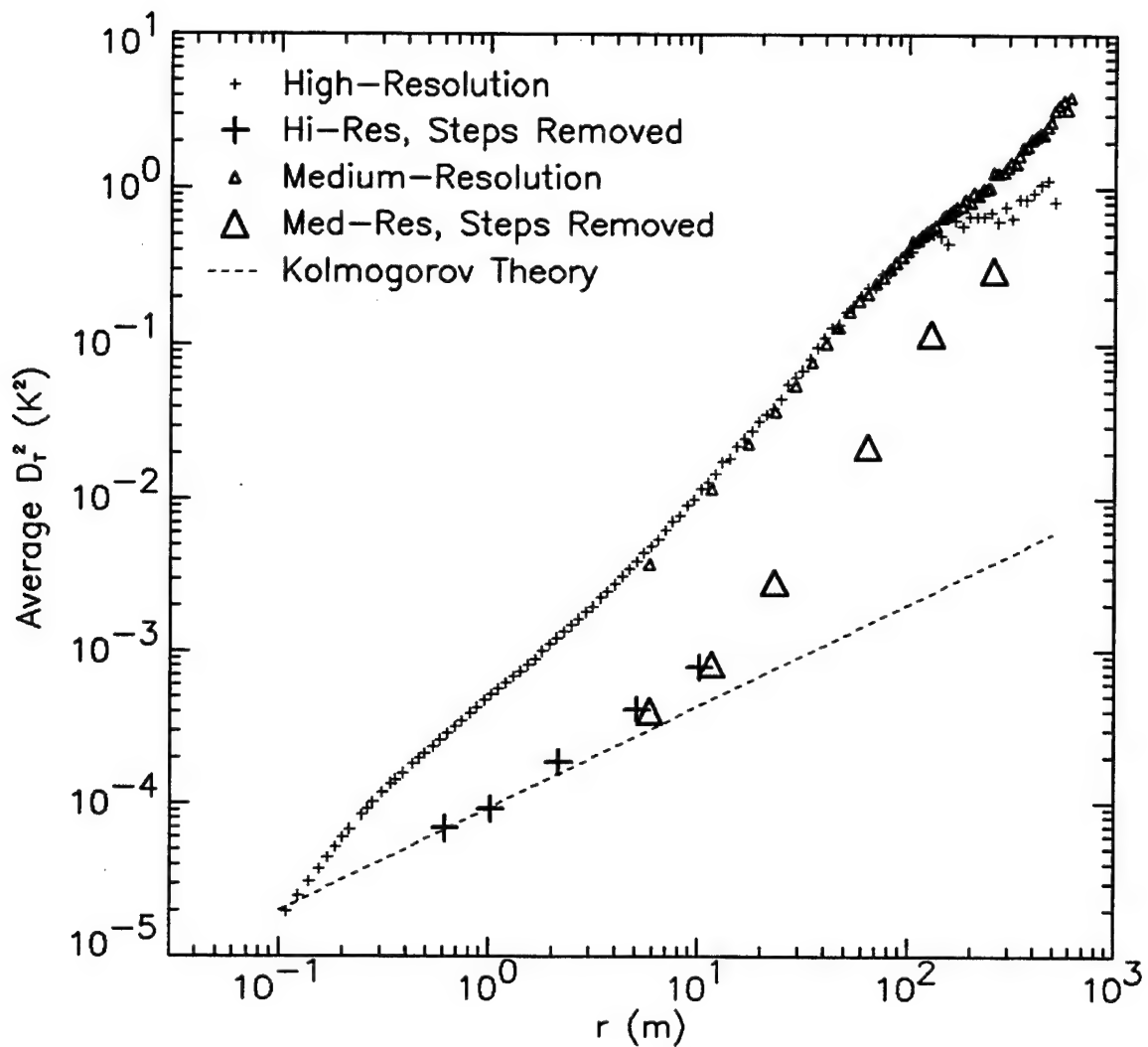
Figure 13. Average 2nd order structure function of the high-resolution temperature profile in the stratosphere (10.4-19.4 km) plotted against sampling interval. Results of step removal follow the Kolmogorov theoretical 2/3 slope until ~10 m. High and medium-resolution data match well.
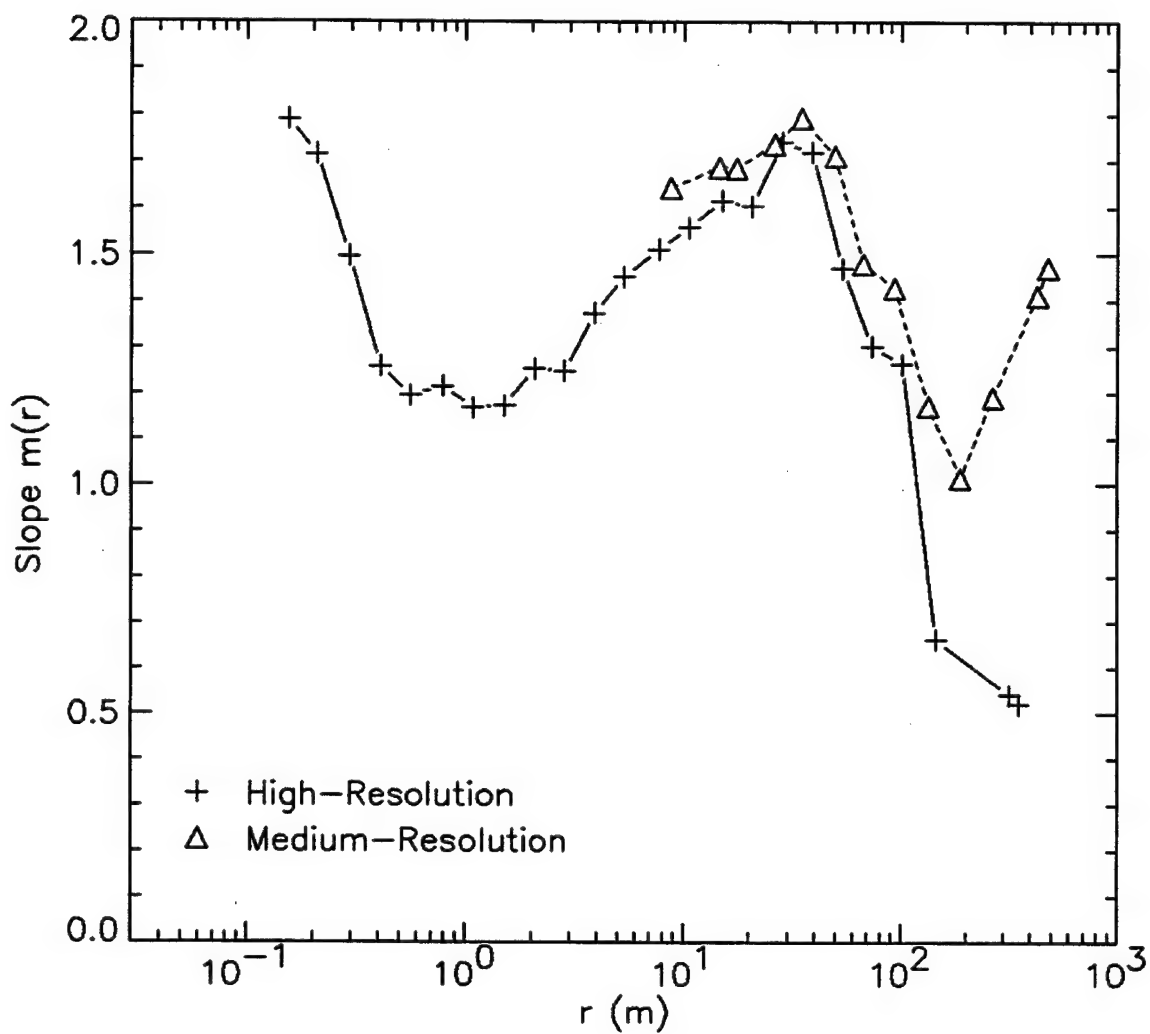
Figure 14. Slope of the 2nd order structure function plotted against sampling interval. High and medium-resolution slopes match well below 100 m.

37

evidence of the inner scale length, l_0, coupled with the onset of the viscous convective region. Note that the 3 dB point of the thermocouple was at ~4.7 cm. The effects of dissipation were quite significant below ~25 cm, a value for which the slope has risen halfway from the flat region of the curve to the theoretical value of 2. This marks the inner scale of the inertial subrange and corresponds to ~20 Hz on the power spectrum in Figure 12. Averaging the stratosphere smears the inner scale effect because the inner scale grows with decreasing pressure at higher altitudes.

The slope falls rapidly with r until reaching a plateau from 0.5 m to 2 m. A steady rise in slope above 1 m indicates the contribution of step discontinuities to the structure function. Apparently, the steps prevented the slope from ever reaching 2/3. The Q ratio of Equation (25) predicted an increase in the effective exponent, $m(r)$. It was expected that the slope would rise to about 2 and level off when steps produced the majority of the structure. The fact that it did not do so implies the step effect was reduced above 40 m. This behavior may characterize the maximum size of small steps. The rise in slope beyond 200 m possibly indicates a regime of large steps. The analysis is limited for large r because the number of values used in the average declines inversely with r.

B.   REMOVAL OF STEPS

From the behavior of $D^{(2)}_T(r)$, it was initially concluded there was no Kolmogorov inertial subrange along a vertical profile of the stratosphere. Based upon the

theory of steps presented in Chapter II, an attempt was made to eliminate their contribution to the structure function. The 2nd and higher order structure functions mathematically fail in the presence of rapid slope changes or temperature steps, leading to a criterion for their identification. Visual judgement by the investigator determined the presence of reasonably obvious slope changes that could not be random turbulence. The rapid slope change across the step temperature increase in Figure 9 is an example at 5 m resolution. At 100 m resolution this particular step was not resolved and did not cause a significant shift in the slope. The change in slope was very gradual at the minimum useable data resolution of 9.24 cm, therefore this step was not removed. The main vertical extent of the turbulent sheets in the stratosphere ranges from meters to tens of meters (Dalaudier, 1994). Only the top and bottom edges of these sheets were deemed steps and removed by this procedure, leaving the middle of the sheet intact when the sampling interval permitted.

The steps were identified for several selected sampling intervals for both instruments, listed in Table 1. The investigator manually viewed every data point

High-Resolution		Medium-Resolution	
r (m)	C_T^2 ($K^2 m^{2/3}$)	r (m)	C_T^2 ($K^2 m^{2/3}$)
0.62	0.944e-4	5.82	1.24e-4
1.02	0.903e-4	11.6	1.59e-4
2.16	1.11e-4	23.3	3.47e-4
5.08	1.39e-4	64.0	13.8e-4
10.2	1.67e-4	127.9	46.2e-4
		255.9	74.0e-4

Table 1. Results of step removal.

at each of the selected r values and flagged the affected regions. All flagged data were replaced with the local logarithmic average in the manner of processing the interference spikes in Chapter III. Uncertainty in C_T^2 is reduced by the 3/5 power when calculating the optical parameters r_0, θ_0, and f_g. Complexity of developing an automated algorithm along with limited time necessitated a manual procedure. The Q value could prove useful in developing an automated routine by defining a maximum permitted value, Q_{max}. The maximum allowable slope difference would then be,

$$B_{max} = \left[2.41 C_T^2 Q_{max}\right]^{1/2} r^{-2/3}.$$
(31)

Figure 15 is a comparison of the C_T^2 profiles after step removal for the 5.08 m high-resolution and 5.82 m medium-resolution cases, with 250 m smoothing for visualization. The profiles agree well except above 18 km, where both probes produced a similar turbulence spike at 18.5 km, although offset by roughly a factor of 3. Excessive manual step removal in the medium-resolution profile was most likely the cause of this discrepancy. In addition, there is a good correlation between high turbulence and the strong wind shear regions in Figure 7. The pre and post step-removal dependence of C_T^2 on r is shown in Figure 16. The two leftmost step values were averaged to obtain $\langle C_T^2 \rangle$ =0.924e-4 ($K^2 m^{2/3}$). These two points were chosen because they appeared to represent an asymptotic limit of the step removal process. It is interesting that this value
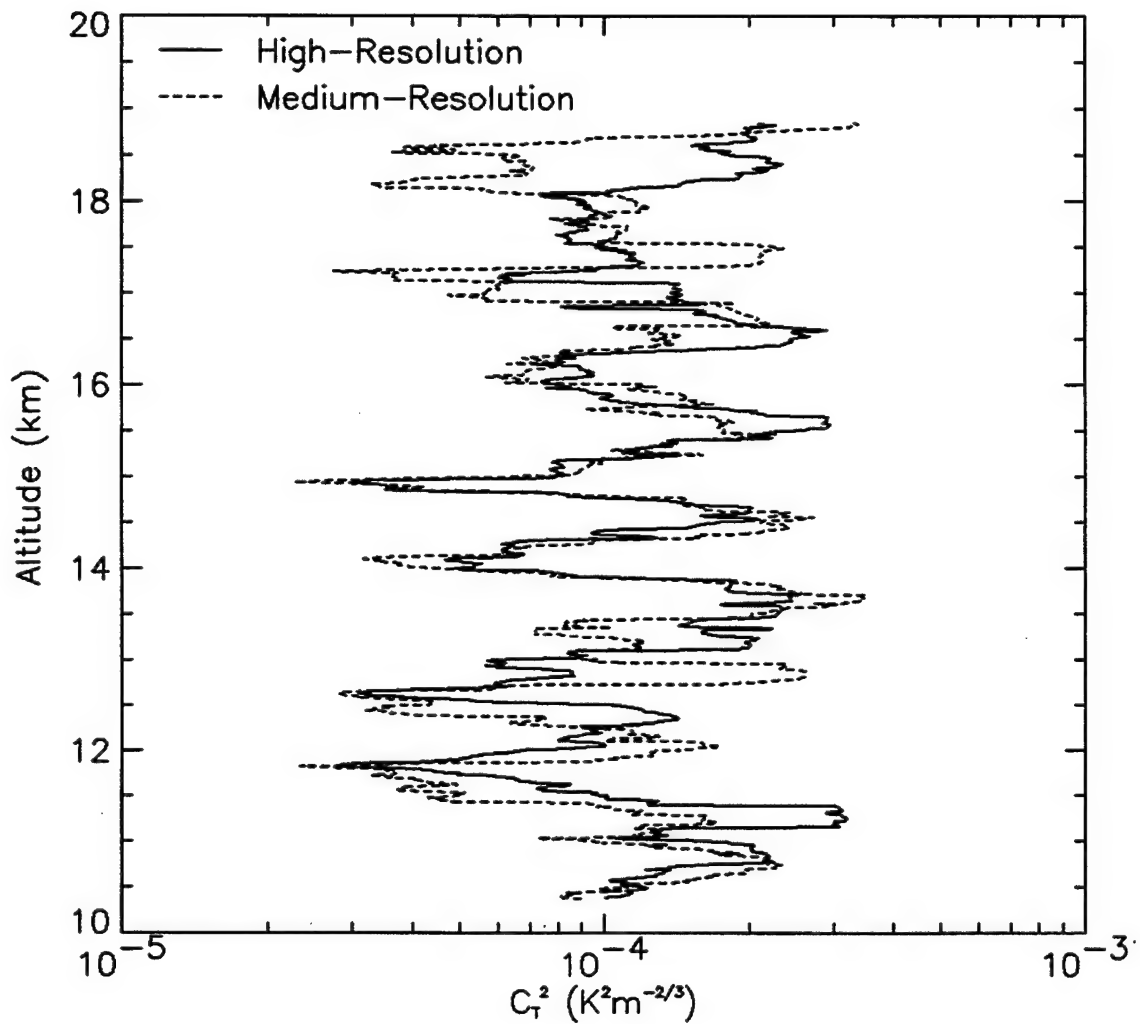
Figure 15. Turbulence parameter in the stratosphere plotted against altitude. The steps were removed for sampling interval $r = 5.08$ m for high-resolution and $r = 5.82$ m for medium-resolution. High and medium-resolution profiles match well below 18 km. A 250 m smoothing filter was applied for visualization.

Figure 16. Average turbulence parameter in the stratosphere (10.4-19.4 km) plotted against sampling interval. Manual removal of steps was performed for 11 sampling intervals. The curve formed by these points has an asymptotic value of 9.24e-5 for the turbulence parameter. The approximately constant region corresponds to a Kolmogorov inertial subrange with outer length scale $L_0 \sim 10$ m.

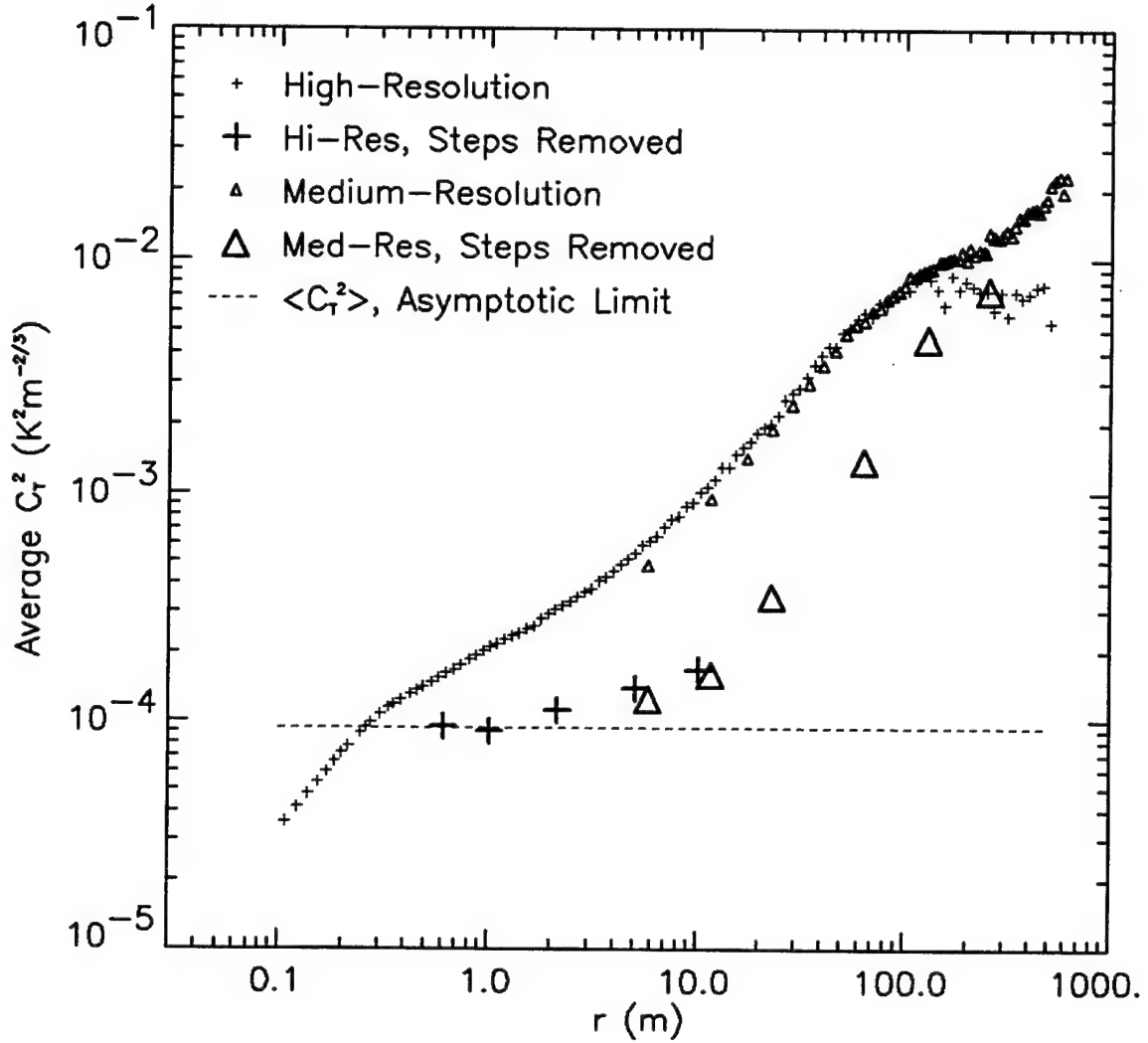intersects the unprocessed curve at ~25 cm. The step-removed values depart from a near constant value above 10 m, making this an estimate of the outer scale length, L_0, of the Kolmogorov inertial subrange. The step removed $D^{(2)}{}_T(r)$ values plotted in Figure 13 also depart noticeable from the 2/3 theoretical slope above 10 m.

The four bends in Figures 13, 14, and 16 summarize the physics of the atmosphere for this balloon launch. The bend at 25 cm marks the inner scale boundary between the dissipation regime and the inertial subrange. A bend at 3 m marks the scale where temperature steps become the dominant source of structure and steadily grow in importance, according to the Q ratio in Equation (24). Steps came into play at small r, before a Kolmogorov inertial subrange could be established. The decrease in slope at 40 m characterizes a scale length above which step effects declined. A final increase in slope at 200 m indicates an increase in the steps, although the statistics are not as good for this range of sampling intervals. This could indicate that the distribution of step sizes has multiple modes, with a gap between 40 m and 200 m.

Removal of steps revealed an underlying outer scale length, L_0~10 m. Below L_0, the procedure uncovered a nearly Kolmogorov inertial subrange. Earlier research noted that $C_T{}^2$ from a high-resolution vertical profile, $r=1$ m, was a factor of ~1.6 greater than that measured by a 1 m horizontal pair of temperature probes (Walters, 1995). Figure 16 predicts a factor of ~2. Since horizontally spaced probes are also susceptible to steps, from pendulum motion of the package under the balloon in the presence of vertical slopes in the stratified layer, this investigation indicates 1 m horizontally spaced probes over-

predict turbulence by perhaps 10-25%. The inability of horizontal probes to measure a horizontal temperature profile makes the step removal process impossible with current systems. The application of a correction factor is unwarranted without further research to quantify the factor more accurately.

The results are based upon the stratosphere only, but the theory should also be applicable to the troposphere. Current meteorological weather balloons, with the addition of an inexpensive bead thermistor, would yield a temperature profile of ~5 m vertical resolution, though 1-2 m would be preferred. Under lower turbulence conditions than this investigation, the stratified temperature profile would be less disturbed and the step contribution is expected to be lower; the procedure should continue to work. Higher turbulence is expected to raise the outer scale length, while simultaneously increasing the effect of steps. Further research should reveal which of these two competing effects dominates and show if a 5 m vertical resolution temperature profile is sufficient for a wide range of atmospheric conditions.

V. CONCLUSIONS

Spatial variations in the index of refraction of the atmosphere distort propagating electromagnetic waves. Many laser and telescope systems of interest to the military operate within the visible through near infrared portion of the spectrum and are susceptible to these effects. The effects of atmospheric turbulence are the primary limitation to performance of high angular resolution systems. The Air Force's Airborne Laser program and other military adaptive optics systems would benefit from the ability to forecast severe atmospheric turbulence situations accurately. Good validation data is required to develop such a model.

Structure functions provide a robust means of extracting the index of refraction structure constant, C_n^2, a useful turbulence parameter in the atmosphere. Vertical temperature profiles through the atmosphere reveal the presence of steps in the potential temperature. The rapid change in slope of the temperature across these steps contributes a false term to C_n^2. This research developed a quantitative measure of the false turbulence contribution caused by the temperature slope discontinuities in the atmosphere. The homogeneity and isotropy requirements of structure functions led to a technique of removing the false contribution.

Both 1.54 cm and 5.82 m vertical resolution profiles of temperature were collected from a balloon flight in March 1995 from Wichita, Kansas. Data processing removed and compensated for interference spikes in the high-resolution temperature profile. Treating the stratosphere as an ensemble average, the application of a second-

45

order structure function to the temperature profiles confirmed the presence of a temperature step contribution. Removal of the temperature steps for several sampling intervals exposed a Kolmogorov inertial subrange extending from ~25 cm to ~10 m.

The results were based upon the stratosphere only, but the theory should be applicable to the troposphere, where the temperature steps are less pronounced. Future research could extend the analysis to the troposphere. Current meteorological weather balloons, with slight modification, are capable of measuring temperature profiles with 5 m vertical resolution. Based upon the results of others, wind shear appears to be the source of the steps (Bertin, 1997) (Dalaudier, 1994). The effect of these steps should be less pronounced under lower turbulence conditions, and the procedure should continue to work. Higher turbulence is expected to raise the outer scale length while simultaneously increasing the magnitude or number of steps. Further research should decide if 5 m vertical resolution is sufficient for a wide range of turbulence conditions.

This investigation produced a reference turbulence profile in the stratosphere for validation of turbulence forecasting models. The potential of this technique to compute the isoplanatic angle, θ_0, coherence length, r_0, and Greenwood frequency, f_g, reliably with inexpensive balloons should benefit ABL and other national programs.

LIST OF REFERENCES

Bertin, F., J. Barat, and R. Wilson, "Energy Dissipation Rates, Eddy Diffusivity, and the Prandtl Number: An in Situ Experimental Approach and its Consequences on Radar Estimate of Turbulent Parameters", *Radio Science*, Vol. 32, pp. 791-804, 1997.

Coulman, C. E., J. Vernin, and A. Fuchs, "Optical Seeing-Mechanism of Formation of Thin Turbulent Laminae in the Atmosphere", *Applied Optics*, Vol. 34, No. 24, pp. 5461-5474, 1995.

Dalaudier, F., C. Sidi, M. Crochet, and J. Vernin, "Direct Evidence of "Sheets" in the Atmospheric Temperature Field", *Journal of The Atmospheric Sciences*, Vol. 51, No. 2, pp. 237-248, 1994.

Fried, D. L., "Optical Resolution Through a Randomly Inhomogeneous Medium for Very Long and Very Short Exposures," *Journal of the Optical Society of America*, Vol. 56, pp. 1372-1379, 1966.

Fried, D. L., "Anisoplanatism in Adaptive Optics," *Journal of the Optical Society of America*, Vol.72, pp. 52-61, 1982.

Fuehrer, P. L., C. A. Friehe, and D. K. Edwards, "Frequency Response of a Thermistor Temperature Probe in Air", *Journal of Atmospheric and Oceanic Technology*, Vol. 11, pp. 476-488, 1994.

Greenwood, D. P., "Bandwidth Specifications for Adaptive Optics Systems", *Journal of the Optical Society of America*, Vol. 67, pp. 390-393, 1977.

Holton, J. R., *An Introduction to Dynamic Meteorology*, Academic Press, New York, 1979.

Jones, F. E., "The Refractivity of Air", *Journal of Research of the National Bureau of Standards*, Vol. 86, pp. 27-32, 1981.

Roper, D. S., *Investigation of Systematic Effects in Atmospheric Microthermal Probe Data*, Master's Thesis, Naval Postgraduate School, Monterey, California, December 1992.

Tatarski, V.I., *Wave Propagation in a Turbulent Medium*, McGraw-Hill, New York, 1961.

Tennekes, H. and J. L. Lumley, *A First Course in Turbulence*, Massachusetts Institute of Technology, 1972.

Walters, D.L., "Measurements of Optical Turbulence with Higher-Order Structure Functions," *Applied Optics*, Vol. 34, pp. 1591-1597, 1995.

Yaglom, A. M., *Correlation Theory of Stationary and Related Random Functions I and II*, Springer-Verlag, New York, pp. 411-430, 1987.

INITIAL DISTRIBUTION LIST

1. Defense Technical Information Center...2
   8725 John J. Kingman Rd., STE 0944
   Ft. Belvoir, VA 22060-6218

2. Dudley Knox Library...2
   Naval Postgraduate School
   411 Dyer Rd.
   Monterey, CA 93943-5101

3. Curriculum Officer, Code 34...1
   Engineering and Technology
   Naval Postgraduate School
   700 Dyer Road, Room 115
   Monterey, CA 93943-5107

4. Chairman, Code PH...1
   Department of Physics
   Naval Postgraduate School
   Monterey, CA 93943-5101

5. Professor Donald L. Walters, Code PH/We...10
   Department of Physics
   Naval Postgraduate School
   Monterey, CA 93943-5101

6. LT Aaron M. Holdaway..5
   3559 Wall Avenue
   San Bernardino, CA 92404